A Solid-State High-Resolution ^{13}C NMR Study of Octaethylporphyrin and Its Zinc(II) and Nickel(II) Metal Complexes Using CP–MAS Techniques

Masaharu Okazaki and Charles A. McDowell*

Contribution from the Department of Chemistry, University of British Columbia, Vancouver, British Columbia, Canada V6T 1Y6. *Received May 18, 1983*

Abstract: The solid-state high-resolution ^{13}C nuclear magnetic resonance spectra of octaethylporphyrin (OEP) and its Zn(II) and Ni(II) diamagnetic complexes were observed by means of CP–MAS techniques. The observed resonances were assigned by comparison with those of liquid-phase NMR spectra and by the relaxation behavior of each peak. Newly observed extra splittings in the solid-state NMR spectra of OEP are explained by the quenching of the N–H tautomerism among the four pyrrole rings and the intermolecular chemical shielding caused by the ring-current effects, whereas in the case of Zn^{II}(OEP) the observed splitting is explained satisfactorily as arising from the intermolecular ring-current effect. The spectra were simulated by using the isotropic chemical shift values obtained in the solution NMR and another shift calculated by taking account of the intermolecular ring-current effects. The Haigh–Mallion–McWeeny and Johnson–Bovey theories and the dipole method used by Abraham were employed for the calculation of the ring-current effects.

Porphyrins and metalloporphyrins are interesting classes of compounds not only because of their great biological importance but also because of their intrinsic significance in chemistry. Extensive reviews of the NMR studies of diagmagnetic porphyrins and the paramagnetic metalloporphyrins have been reported.[1,2] We are reporting our results of an NMR study of octaethylporphyrin (OEP) and its Zn(II) and Ni(II) diamagnetic complexes in the solid state (Figure 1). To our knowledge, only a few other high-resolution NMR studies of metalloporphyrins in the solid state have been reported.[3]

Solid-state high-resolution ^{13}C NMR spectroscopy involving a combination of cross-polarization, high-power proton decoupling and magic angle spinning (CP–MAS) has been applied to many chemical systems, and such studies have provided much new information.[4–6] In the solid state some degrees of the motional freedom of the molecules are quenched; thus the NMR signals due to conformers and tautomers can be observed separately in many cases.[7,8]

In the NMR spectra of porphyrins in solution sometimes there is a concentration dependence of the chemical shifts; this has been attributed to intermolecular ring-current shielding. Much useful information about the conformations of enzymes having porphyrins as a prosthetic group has been obtained by the analysis of the ring-current shifts for protons in the surrounding groups.[9,10] The quenching of the N–H tautomerism[11–14] has been found in the NMR spectra of porphyrins in solution, at low temperature. These phenomena may be clarified if the ^{13}C solid-state NMR spectrum can be observed with high resolution and at the same time the crystal structure of the porphyrin compound is known.

In this study, the individual NMR resonances observed were assigned by comparison with the solution NMR spectra and by the ^{13}C spin–lattice relaxation behavior of each peak. T_1 (the spin–lattice relaxation time in the Zeeman frame), $T_{1\rho}$ (spin–lattice relaxation time in the rotating frame), and the dipolar dephasing processes[30] were determined for each peak to aid in the assignments. We show that analysis of the spectra, taking into account the calculated intermolecular ring-current shielding,[9,33] can give

(1) (a) Janson, T. R.; Katz, J. J. "The Porphyrins;" Dolphin, D., Ed.; Academic Press: New York, 1979; Vol. 4, Chapter 1. (b) LaMar, G. N.; Walker, F. A. In ref 1a, Chapter 2.

(2) Scheer, H.; Katz, J. J. "Porphyrins and Metalloporphyrins;" Smith, K. M., Ed.; Elsevier: Amsterdam, 1975; Chapter 10.

(3) (a) Jakobsen, H. J.; Ellis, P. D.; Inners, R. R.; Jensen, C. F. *J. Am. Chem. Soc.* **1982**, *104*, 7442. (b) Maciel, G. E.; Shatlock, M. P.; Houtchens, R. A.; Caughey, W. S. *Ibid.* **1980**, *102*, 6885.

(4) Yannoni, C. S. *Acc. Chem. Res.* **1982**, *15*, 201.

(5) Lyerla, J. R.; Yannoni, C. S.; Fyfe, C. A. *Acc. Chem. Res.* **1982**, *15*, 208.

(6) Baliman, G. E.; Groombridge, C. J.; Harris, R. K.; Packer, K. J.; Say, B. J.; Tanner, S. P. *Philos. Trans. R. Soc. London, Ser. A* **1981**, *A299*, 643.

(7) (a) McDowell, C. A.; Naito, A.; Scheffer, J. R.; Wong, Y. F. *Tetrahedron Lett.* **1981**, *22*, 4779. (b) Ganapathy, S.; Naito, A.; McDowell, C. A. *J. Am. Chem. Soc.* **1981**, *103*, 6011.

(8) (a) Dalling, D. K.; Zilm, K. W.; Grant, D. M.; Heeschen, W. A.; Horton, W. J.; Pugmire, R. J. *J. Am. Chem. Soc.* **1981**, *103*, 4817. (b) Saito, H.; Izumi, G.; Mamizuka, T.; Suzuki, S.; Tabeta, R. *J. Chem. Soc., Chem. Commun.* **1982**, 1386. (c) Atalla, R. H.; Gast, J. C.; Sindorf, D. W.; Bartuska, V. J.; Maciel, G. E. *J. Am. Chem. Soc.* **1980**, *102*, 3249. (d) Meier, B. H.; Grab, F.; Ernst, R. R. *J. Chem. Phys.* **1982**, *76*, 767.

(9) (a) Perkins, S. J.; Wuthrich, K. *Biochim. Biophys. Acta* **1979**, *576*, 409. (b) Perkins, S. J.; Dwek, R. A. *Biochemistry* **1980**, *19*, 245. (c) Perkins, S. J. *J. Magn. Reson.* **1980**, *38*, 297.

(10) Perkins, S. J. In "Biological Magnetic Resonance"; Berliner, L. T., Reuben, J., Eds.; Plenum: New York, 1982; Vol. 4, Chapter 4.

(11) Storm, C. B.; Teklu, Y. *J. Am. Chem. Soc.* **1972**, *94*, 1745.

(12) Abraham, R. J.; Hawkes, G. E.; Smith, K. M. *Tetrahedron Lett.* **1974**, 1483.

(13) Abraham, R. J.; Hawkes, G. E.; Hudson, M. F.; Smith, K. M. *J. Chem. Soc., Perkin Trans. 2* **1974**, 204.

(14) Kawano, K.; Ozaki, Y.; Kyogoku, Y.; Ogoshi, H.; Sugimoto, H.; Yoshida, Z. *J. Chem. Soc., Perkin Trans. 2* **1978**, 1319.

(15) McWeeny, R. *Mol. Phys.* **1958**, *1*, 311.

(16) Haigh, C. W.; Mallion, R. B. *Mol. Phys.* **1971**, *22*, 955.

(17) Pople, J. A. *J. Chem. Phys.* **1956**, *24*, 1111.

(18) Abraham, R. J. *Mol. Phys.* **1961**, *4*, 145.

(19) Abraham, R. J.; Bedford, G. R.; NcNeillie, D.; Wright, B. *Org. Magn. Reson.* **1980**, *14*, 418.

(20) Waugh, J. S.; Fessenden, R. W. *J. Am. Chem. Soc.* **1957**, *79*, 846.

(21) Johnson, C. E., Jr.; Bovey, F. A. *J. Chem. Phys.* **1958**, *29*, 1012.

(22) For review; Haigh, C. W.; Mallion, R. B. *Prog. Nucl. Magn. Reson. Spectrosc.* **1980**, *15*, 303.

(23) For the more rigorous treatment, the contribution of the atomic diamagnetic anisotropies should be considered. See: Salem, L. "Molecular Orbital Theory"; Benjamin: New York, 1965.

(24) Pauling, L. *J. Chem. Phys.* **1936**, *4*, 673.

(25) London, F. *J. Phys. Radium* **1937**, *8*, 397.

(26) Abraham, R. J.; Smith, K. M.; Goff, D. A.; Lai, J. *J. Am. Chem. Soc.* **1982**, *104*, 4332 and references therein.

(27) Abraham, R. J.; Plant, J.; Bedford, G. R. *Org. Magn. Reson.* **1982**, *19*, 204 and references therein.

(28) Lauber, J. W.; Ibers, J. A. *J. Am. Chem. Soc.* **1973**, *95*, 5148.

(29) A volume containing 27 unit cells is adequate in this case. The next larger volume containing an additional 98 unit cells; These contribute only 2% at most. Because of the r^{-3} dependence of this mechanism, and also since we are only concerned about the variation of the ring-current shifts in a particular molecule, the contribution from an outer shell at a distance much greater than the molecular diameter from the center of a particular molecular can be neglected. (The outer shell causes the same ring-current shifts for all the nuclei in the central molecule under consideration.)

(30) Opella, S. J.; Frey, M. H. *J. Am. Chem. Soc.* **1979**, *101*, 5854.

(31) Meyer, E. E., Jr. *Acta Crystallogr., Sect. B* **1972**, *B28*, 2162.

(32) Alla, M.; Lippmaa, E. *Chem. Phys. Lett.* **1982**, *87*, 30.

0002-7863/84/1506-3185$01.50/0

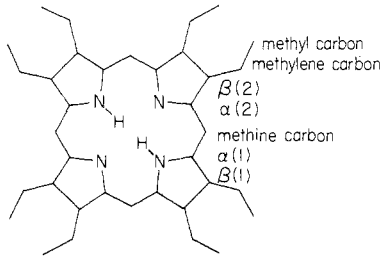

Figure 1. Structure of octaethylporphyrin (OEP) showing the labeling of the atoms.

information about the degree of symmetry of the crystal structure of porphyrins. We have employed the Haigh–Mallion–McWeeny (HMM) theory,[15,16] Abraham's 16-dipole method,[17,18] and the Johnson–Bovey theory (JB)[20,21] to calculate the intermolecular ring-current effects in the solid-state ^{13}C NMR spectra of OEP and Zn^{II}(OEP). These calculations enabled us to make computer simulations of the predicted spectra for the latter compounds. Comparing the theoretically simulated spectra with those determined experimentally confirmed our spectral assignments. The splitting constant due to the quenching of the N–H tautomerism was determined by comparison of the simulated and the experimental CP–MAS spectrum of OEP.

Experimental Section

Octaethylporphyrin (OEP) and its complexes with Zn(II) and Ni(II) were kindly supplied by Professor David Dolphin of this department. The CP–MAS ^{13}C NMR spectra, with proton decoupling, were obtained by using a Bruker CXP-200 spectrometer operating with resonance frequencies of 200 MHz for ^{1}H and 50.3 MHz for ^{13}C nuclei, respectively. The single contact cross-polarization pulse sequence was used under the Hartman–Hahn condition, which was established by applying ^{1}H and ^{13}C resonance rf fields of 10 and 40 G, respectively. The contact and repetition times were chosen to be 5 ms and 4 s, respectively. All experiments were carried out at room temperature.

The spin–lattice relaxation T_1 values were determined by the saturation recovery method. The width of the presaturation pulse was 3 ms, and the amplitude was 40 G. The $T_{1\rho}$ measurements were performed by inducing the ^{13}C magnetization by cross-polarization, which was then spin-locked by a locking pulse followed by the proton decoupling pulse while the ^{13}C free induction decay was monitored.

A Delrin spinner was used in the experiments for the T_1 measurements. In other cases, a deuterated Plexiglas spinner was used. The spinning frequencies were 4.2 and 3.7 kHz for the Delrin spinner and the Plexiglas spinners, respectively. One thousand and two thousand transients were accumulated for each spectrum to provide acceptable accuracy in the $T_{1\rho}$ and T_1 measurements, respectively. Solution NMR were obtained by using a Bruker WH-400 spectrometer. The concentration of the solute was about 2.0×10^{-3} mol L^{-1}, and no additives were employed to prevent aggregation of the metal complexes or to increase the solubilities.

Ring-Current Theories and Computation Methods

Ring-current theories[22,23] are based on either the Pauling classical theory,[24] which attempted to account for the anisotropic magnetic susceptibility of aromatic hydrocarbons, or London's quantum mechanical theory,[25] which attempted to give a more fundamental interpretation. Pople used the equivalent dipole approximation of the circulating π-electron current to explain the origin of the proton chemical shifts observed in aromatic compounds.[17] Following Pople's work, a classical current loop theory was described by Johnson and Bovey.[20,21] Subsequently an extensive quantum mechanical theory was put forward by Haigh and Mallion,[16] who based their work on earlier theoretical studies by McWeeny.[15] Abraham has extended the Pople equivalent dipole method to attempt to account for the observed proton and ^{13}C chemical shifts of a wide number of porphyrin compounds in solution.[18,26,27]

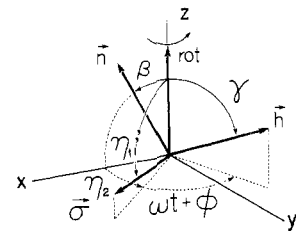

Figure 2. Coordinate system for the averaging of the Hamiltonian in the MAS experiments.

The equivalent dipole moment points in the direction n, which is normal to the aromatic plane. Its magnitude is proportional to the applied magnetic field B_0. Thus, the interaction energy between the nuclear magnetic moment m_1 and the equivalent dipole moment becomes

$$E_d = (m_1 B_0 C S \mu_0 / r^3)(\vec{n}\cdot\vec{h})((\vec{n}\cdot\vec{h}) - 3\,(\vec{n}\cdot\vec{\sigma})(\vec{\sigma}\cdot\vec{h})) \quad (1)$$

where C is a constant that depends on the strength of the ring current, S is the area of the ring, μ_0 is the magnetic susceptibility, $\vec{h}$ is the unit vector in the direction of the magnetic field, and r is the distance between the two dipoles. $\vec{\sigma}$ represents the unit vector associated with the vector $\vec{r}$ which connects the two dipoles.

In the liquid phase the molecule rotates isotropically; thus eq 1 becomes

$$E = [m_1 B_0 C S \mu_0 / 3r^3](1 - 3\cos^2\alpha) \quad (2)$$

In Abraham's 16-dipole method for porphyrins, each dipole is located at a distance z_D above, or beneath, the aromatic plane. The equation for the isotropic ring-current shift δ, in units of ppm, deduced from eq 2 is

$$\delta \times 10^{-6} = \sum_i \mu_1(1 - 3(z_i \pm z_D)^2/r_i^2)/r_i^3 + \sum_j \mu_2(1 - 3(z_j \pm z_D)^2/r_j^2)/r_j^3 \quad (3)$$

where μ_i is the ring-current factor, which is defined as $\mu_i = m_1 C S_i \mu_0/3$, and z_i is the z component of r_i in the molecular coordinate system. The summation is taken over the 16 dipoles.

In the case of the MAS experiment in the solid state, a different procedure for the averaging must be followed. In Figure 2 the coordinate system for this purpose is depicted. The expressions for $(\vec{n}\cdot\vec{h})$, $(\vec{n}\cdot\vec{\sigma})$, and $(\vec{h}\cdot\vec{\sigma})$ are as follows:

$$(\vec{n}\cdot\vec{h}) = \sin\beta\sin\gamma\cos(wt + \phi) + \cos\beta\cos\gamma$$

$$(\vec{n}\cdot\vec{\sigma}) = \sin\beta\sin\eta_1\cos\eta_2 + \cos\beta\cos\eta_1$$

$$(\vec{h}\cdot\vec{\sigma}) = \sin\gamma\sin\eta_1\cos(wt + \phi - \eta_2) + \cos\eta_1\cos\gamma \quad (4)$$

By substitution from eq 4 into eq 1 and use of the relation $\cos^2\gamma = {}^1/_3$, eq 1 becomes eq 2. Thus, eq 3 also can be applied to the case of the MAS experiment on porphyrins in the solid state.

In the Johnson–Bovey method[21] the secondary field B_h is expressed as follows:

$$B_h = B_n\cos\theta + B_\rho\sin\theta \quad (5)$$

The subscripts n and ρ represent the z component, and the ρ component of the cylindrical coordinate system. θ is defined by $\cos\theta = \vec{n}\cdot\vec{h}$. The ring-current shift in the solid state thus can be expressed as

$$\delta \times 10^{-6} = B_h/B_o = (B_n\cos^2\theta + B_\rho\sin\theta\cos\theta)/B_o \quad (6)$$

where

$$B_n = 2I/\{[(a+\rho)^2 + z^2]^{1/2}\}\{K + E(a^2 - \rho^2 - z^2)/[(a-\rho)^2 + z^2]\}$$

$$B_\rho = 2Iz/\{[(a+\rho)^2 + z^2]^{1/2}\} \times \{-K + E(a^2 + \rho^2 + z^2)/[(a-\rho)^2 + z^2]\}$$

where δ is the component of the chemical shift tensor δ along the direction of applied field $B_0\vec{h}$ and a, z, and ρ represent the radius

(33) (a) Giessner-Prettre, C.; Pullman, B. *J. Theor. Biol.* **1971**, *31*, 287. (b) Giessner-Prettre, C.; Pullman, B. *Biochem. Biophys. Res. Commun.* **1976**, *70*, 578. (c) Giessner-Prettre, C.; Pullman, B. *Ibid.* **1981**, *101*, 921.

(34) Agragam, A. "The Principle of Nuclear Magnetism"; Clarendon Press: Oxford, 1961.

of the ring, the coordinate associated with $\vec{n}$, and the coordinate associated with $\vec{\rho}$, respectively. The modulus k of the complete elliptic integral K (first kind) and E (second kind) is expressed by

$$k^2 = 4a\rho/[(a+\rho)^2 + z^2] \quad (7)$$

In the case of solution NMR, after averaging with respect to time, eq 6 becomes

$$\delta \times 10^{-6} = B_n/3 = J\{K + E(a^2 - \rho^2 - z^2)/[(a-\rho)^2 + z^2]\}\{(a+\rho)^2 + z^2\}^{-1/2} \quad (8)$$

In the MAS experiment, as was shown in the section on the dipole method, the averaged value of $\cos^2\theta$ is equal to $^1/_3$. The second term of eq 6, however, cannot be averaged out in contrast to the case of solution NMR. According to the coordinate system shown in Figure 2, the second term of eq 6 can be modified as

$$B_\rho \cos\theta \sin\theta = B_\rho\{\sin 2\gamma\ (1 - 3\cos^2\eta_1)/4.0 + f(t)\} \quad (9)$$

where $f(t)$ becomes zero after averaging over time, t. The first term of eq 9 gives the line-width broadening because the averaged value with respect to the space coordinate is zero.

We have also used the HMM quantum mechanical theory[16] to calculate the theoretical values for the chemical shifts as porphyrins. In this theory the concluding equation is as follows:

$$\delta \times 10^{-6} = -2\beta(e/c\hbar)^2(\vec{n}\cdot\vec{h})^2[\sum_{ij} P_{ij}(S_{ij}^{P})^2 k_{ij} + \sum_{ij}\sum_{kl} \beta/2\pi_{ij,kl} S_{ij}^{P} S_{kl}^{P}(k_{ij} + k_{kl})] \quad (10)$$

where S_{ij}^{P} is the signed area of triangle $\widehat{Oij}^{P}$, which is obtained by projecting the triangle $\widehat{Oij}$ to the molecular plane. Here O means the origin of the coordinate where the nucleus under consideration is located, and i and j are the symbols for the component atoms that form the aromatic ring. P_{ij} and $\pi_{ij,kl}$ represent the bond order of ij bond and the imaginary part of the mutual polarizability of the ij and kl bonds, respectively. k_{ij} in eq 10 is the geometrical factor which is approximated as

$$k_{ij} = (1/r_i^3 + 1/r_j^3) \quad (11)$$

In the liquid phase as well as in the MAS experiment in the solid phase the isotropic value of the chemical shift tensor δ can be obtained by replacing $(\vec{n}\cdot\vec{h})^2$ with $^1/_3$ in eq 10. According to MeWeeny, eq 10 can be further simplified to eq 12,[15,16] where

$$\delta \times 10^{-6} = (-2B/3)(e/c\hbar)^2 \sum_{\mu} J'_{\mu}(-K(r_\mu)) = \sum_{\mu} J_\mu(-K(r_\mu)) \quad (12)$$

J_μ is the ring-current factor of ring μ and $K(r_\mu)$ is a geometric factor, which is represented by eq 13. Another term that con-

$$K(r_\mu) = \sum_{(ij)} S_{ij}^{P} k_{ij} \text{ (ordered sum for the ring } \mu) \quad (13)$$

tributes only to the line width and corresponds to eq 9 also arises if we consider the nondiagonal parts of the chemical shift tensor δ.

We simulated the observed solid-state ^{13}C CP–MAS spectra by taking the following factors into account: (a) the intramolecular contribution of the chemical shift was assumed to be equal to that of the spectrum observed in the liquid phase; (b) the intermolecular contribution was calculated by the three theories of the ring-current effects mentioned above; (c) for OEP the quenching of the N–H tautomerism was included; (d) each line is broadened to the appropriate amount by assuming a Lorentzian line shape function. The parameters for processes a–d were varied until we obtained simulated spectra which agreed well with the experimental ones.

OEP crystals with the space group $P_{\bar{1}}$ symmetry have only one molecule per unit cell.[28] To evaluate the intermolecular ring-current shift to a reasonable degree of accuracy, we calculated the interaction in a volume of the crystal lattice consisting of 27 unit cells.[29] In the case of the 16-dipole method, eq 3 was used, with μ_1 and μ_2 as the adjustable parameters. z_D is set equal to 0.64 Å following Abraham et al. Equation 8 was used for the JB method. Equations 11 and 12 were used for the HMM method and the ring-current factors (J_μ) treated as adjustable parameters. The calculation of the geometrical factor was carried out in units of angstroms (see Table III) in the triclinic coordinate system (see Appendix).

Table I. Second Moments of the Nuclei Shown in Figure 1[a]

C nucleus	2nd moment[b]
α(1)	0.244
α(2)	0.136
β(1)	0.297
β(2)	0.292
methine	7.253
methylene	13.29
methyl	2.593

[a] These values are represented in units of 10 (rad/s)^2. [b] The angular dependent term in the Van Vleck formula (ref 34, Chapter 4, eq 55) is calculated by averaging with respect to the magic angle sample spinning and over the directions of microcrystals, i.e., $(1-3\cos^2\theta)^2 = {}^4/_5$). The contribution from the methyl protons is calculated by using the averaged dipolar Hamiltonian (ref 34, Chapter 10, eq 65) with respect to the rotation along the C_3 axis of the methyl group.

The adjustable parameter J, in both the HMM and the JB methods, corresponds with the classical electric current, μ in the 16-dipole method, however, corresponds with the classical magnetic shell. Care must be taken when the parameters of the various models are compared.

Results and Discussion

Peak Assignment. OEP. The solid-state ^{13}C CP–MAS NMR and solution ^{13}C NMR spectra of OEP are shown in Figure 3a. We assign peaks A, B, and C to the pyrrole carbon atoms and peak D to the methine carbon of the macro ring; peaks E, F, and G are assigned to the ethyl group carbon atoms. The observed T_1 values for peaks A, B, and C are 27.1, 20.9, and 19.9 s, respectively. Peak F has two time constants, 1.0 and 7.5 s; the former may be assigned to the methyl carbon and the latter to the methylene carbon atom. The peak of the α-carbon atom should be split into two because of the quenching of the N–H tautomerism. Peak A, at the lowest field, is assigned to one of the group of α-carbon atoms. This assignment is made because the T_1 value of the α-carbon atoms is expected to be greater than that of the β-carbon atoms, because the former has a smaller second moment and also it is more distant from the rapidly rotating methyl group.

It is not clear at this stage if the other peak for the α-carbon is peak B or peak C. The results of the $T_{1\rho}$ measurements show that the heights of peaks B and C collapse more rapidly than does peak A, and finally the heights of peaks A and C become equal. The $T_{1\rho}$ values at the low locking field of the ^{13}C nuclei which are located in a similar dynamical environment are determined by the second moment M_{CH}^2. Thus, from the M_{CH}^2 values shown in Table I, the relation $T_{1\rho}$ (α-carbon) > $T_{1\rho}$ (β-carbon) > $T_{1\rho}$ (methine) is expected. It is also expected that $T_{1\rho}$ (methyl) > $T_{1\rho}$ (methylene). Therefore, the rapidly decaying peaks in the pyrrole region, i.e., peak B and one component of peak C, can be assigned to the β-carbon and the remaining one to the α-carbon. In the ethyl region of the spectrum, the rapidly decaying part of peak F in the $T_{1\rho}$ experiment is assigned to the methylene carbon, and the rest to the methyl carbon atoms.

To obtain further information about the relaxation behavior of the carbon atoms in this ethyl region, the spectra shown in Figure 4 were obtained by using the pulse sequence devised by Opella et al.[30] In this experiment, the components that have stronger dipolar coupling with protons disappear faster when an interval is provided that allows the ^{13}C magnetization to decay, before the data acquisition is begun. Thus, the methylene signal disappears faster than the methyl signal. So in Figure 4B there should be no signals due to the methylene carbon atom. The observed triplet whose intensity ratio is about 1:2:1 in the spectrum shown in Figure 4B is due to the methyl carbon alone. The position of the shoulder observed in the ethyl region of the

Table II. Chemical Shifts in the Solid-State ^{13}C CP-MAS NMR and the Solution NMR Spectra of Three Porphyrins[a]

		Cα	Cβ	meso	ethyl
OEP	solid	149.9	142.3	94.9	21.3, 18.1
		137.0	137.0		14.0
	liquid	144.2	141.5	96.5	19.9, 18.5
Zn^{II}(OEP)	solid	143.9	140.0	94.1	19.3, 17.3
			136.4		
	liquid	148.0	143.0	97.9	20.2, 18.8
Ni^{II}(OEP)[b]	solid	140.4	140.4	95.9	20.1, 20.1
	liquid	143.1	141.0	97.4	20.1

[a] δ from Me_4Si. [b] Single peak is observed in the pyrrole region as well as in the ethyl region.

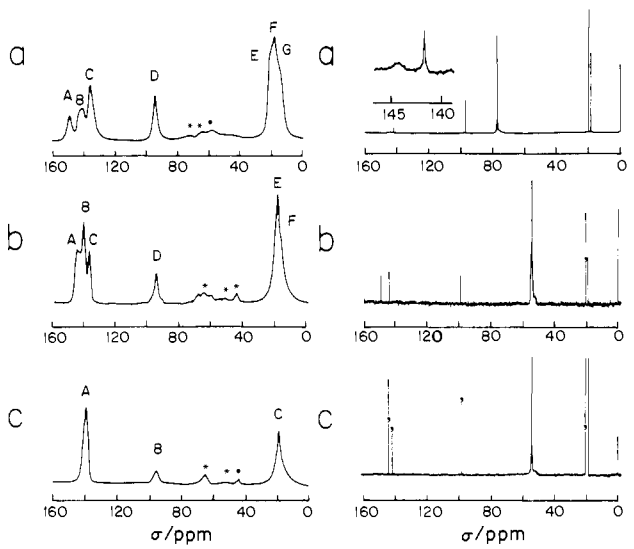

Figure 3. Solid-state ^{13}C CP-MAS NMR and solution NMR spectra of OEP free base, Zn^{II}(OEP), and Ni^{II}(OEP). Signals labeled with an asterisk are the spinning side bands and the absorption peaks from the spinner. Signals at about 77 and 54 ppm in the solution NMR spectrum from the solvent $CDCl_3$ and CD_2Cl_2, respectively.

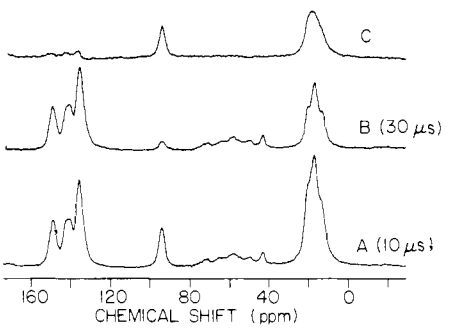

Figure 4. Signals obtained after different periods of the dipolar decay in the ^{13}C CP-MAS NMR spectrum of OEP: (A) after 10-μs dipolar decay; (B) after 30-μs decay; (C) difference between (A) and (B).

spectrum shown in Figure 4A coincides with the position of this triplet, and, therefore, in the difference spectrum Figure 4C the signal in this region is assigned to the methylene carbon atoms.

Zn^{II}(OEP). Solid-state ^{13}C CP-MAS NMR and ^{13}C solution NMR spectra are shown in Figure 3b. Each group of peaks is roughly assigned by the comparison between the two spectra in Figure 3b. Thus, peaks A, B, and C are assigned to the pyrrole carbon atoms, and peaks D and E (and the shoulder F) are assigned to the methine and the ethyl carbon atoms, respectively.

To obtain further detailed assignments, the $T_{1\rho}$ experiments were employed. In the pyrrole region, peak A has a much longer $T_{1\rho}$ value than those of peaks B and C. This fact indicates that peak A should be assigned to the α-carbon and peaks B and C to the β-carbon because of the relative values of M_{CH}^2 shown in Table I. This assignment is also supported by the chemical shift values of the solution NMR spectrum. The fact that the height

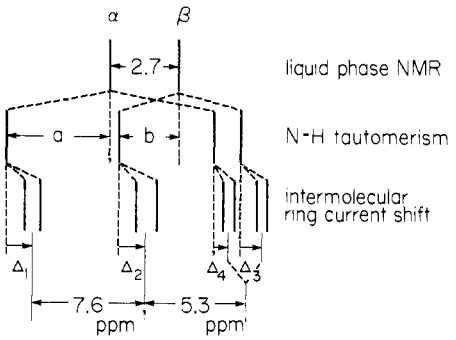

Figure 5. Stick diagram showing the origin of the pyrrole signals in the solid state CP-MAS NMR spectrum of OEP free base. "α" and "β" represent the signals of the α-carbon and β-carbon atoms of the pyrrole ring, respectively. *a* and *b* are the constants representing the splitting caused by the quenching of the N-H tautomerism, and these values are used as the adjustable parameters in simulating the spectrum. Δ_is are the calculated intermolecular ring-current shifts averaged within two chemically equivalent carbon nuclei. Δ_1 and Δ_2 are for the α- and β-carbons of a pyrrole ring with an N-H group, respectively. Δ_4 and Δ_3 are for the α- and β-carbons of a pyrrole ring with a ≥N group, respectively. All the values are expressed in units of ppm.

of peak B is larger than that of peak A means that the linewidth of the α-carbon is much larger than that of the β-carbon. The spectrum of the ethyl region acquired after a 60-μs dipolar decay does not change appreciably from that of Figure 3b. Thus, the peak and the shoulder in Figure 3b are assigned to the methyl carbon exclusively. The signal due to the methylene carbon again should appear as a broad structureless peak.

Ni^{II}(OEP). The solid-state high-resolution NMR and the solution NMR spectra are shown in Figure 3c. In the solid state, the pyrrole region, as well as the ethyl region, appears as a single relatively broad peak. The assignment is quite straightforward. Peak A arises from the pyrrole carbon atoms, peak B from the methine carbon, and peak C from the ethyl carbons. The crystal structure of Ni^{II}(OEP) is $I4_1/a$, and the molecular site has S_4 symmetry.[31] This high symmetry of the system may prevent further splitting in the solid-state NMR spectrum. All the chemical shift values and assignments for the three porphyrins are listed in Table II.

Intermolecular Ring-Current Shift

The major splitting mechanism in the spectrum of the pyrrole region of OEP is from the quenching of the N-H tautomerism. The splitting in the methyl signal, however, cannot be explained by this mechanism because the splitting is a triplet as shown in Figure 4B, rather than a doublet; and besides the magnitude of the splitting is larger than 5 ppm, which is much larger than that expected from the quenching of the N-H tautomerism.

A large splitting is also observed in the signal of the β-carbon of Zn^{II}(OEP) whose pyrrole groups are chemically equivalent. To the best of our knowledge, the crystal structure of Zn^{II}(OEP) is unknown. Thus we cannot exclude the possibility that this splitting may arise from the freezing out of conformers in the solid state. However, the fact that the splitting appears in the signal of the β-carbon, and not in the signal of the α-carbon, cannot be explained by the above mechanisms.

We attribute this newly observed splitting to the intermolecular ring-current shielding.[9,33] It is well-known that very large ring-current shielding effects exist in porphyrins. Thus if the crystal structure of the solid porphyrin has low symmetry, the averaged part of the ring-current interaction for the different carbon atoms may differ from each other.

The chemical shift values for the carbon nuclei were calculated by taking the above mechanism into account and assuming that the isotropic intramolecular shift values are the same as those observed in the solution NMR of the compound.

OEP. A stick diagram which shows the method of simulation of the pyrrole region of the spectrum is shown in Figure 5. As shown in the figure, the signals of both the α-carbon and the β-carbon are split into two peaks by the quenching of the tau-

Table III. List of the Parameters for the Simulation of ^{13}C CP-MAS NMR Spectra[a]

compd	parameters				line width, Hz			
	a	b	$J_1(\mu_1)$	$J_2(\mu_2)$	C_α	C_β	CH_3	CH_2
OEP HMM	7.27	4.75	7.46	12.77	80	70	60	70
JB	7.41	4.73	8.50	11.50	80	70	60	70
16-dip	7.35	4.65	14.0	30.00	80	70	60	70
Zn^{II}(OEP)[b] (pyrrole part)			8.50	11.50	110	55		
(ethyl part)			7.00	2.00			40	70

[a] a and b are given in units of ppm. Care must be taken when comparing our ring-current factors J_1 and J_2 with those in the literature because all our geometrical calculations were carried out in units of angstroms (see text). [b] As mentioned in the text, only the JB method yielded simulated spectra that agreed well with the whole of the observed spectrum. For that reason we do not list the parameters used for the HMM and the 16-dipole methods for this compound.

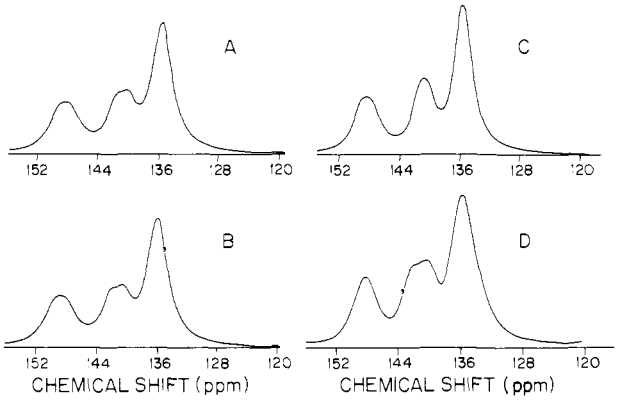

Figure 6. Simulated ^{13}C CP-MAS NMR spectra of the pyrrole region of OEP free base by means of HMM (A), 16-dipole (B), and JB methods (C), and observed spectrum (D). The parameters are given in Table III.

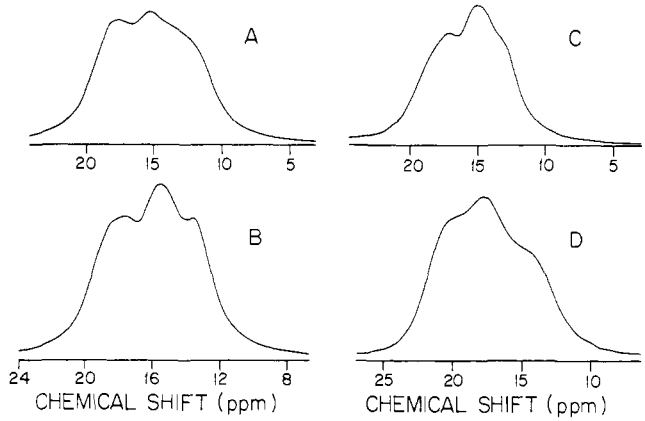

Figure 7. Simulated ^{13}C CP-MAS NMR spectra of the ethyl region of OEP free base and observed one (D). The order of the spectra and the parameters are the same as Figure 3.

tomerism, and each peak is split again into two peaks, and shifts further, by the intermolecular ring-current effects. The signal of the α-carbon in the pyrrole ring which bears the $\geq$N group should appear upfield to that of the α-carbon in the pyrrole group which has the N–H group. The signal of the β-carbon in the pyrrole ring which bears the $\geq$N group should appear at a higher field than that of other β-carbon atoms. The calculated splitting due to the intermolecular ring-current shielding for the β-carbon in the pyrrole ring with the N–H group is much larger than that for the other β-carbon atoms. This conclusion is supported by the fact that there is a small splitting observed in peak B in Figure 3a.

The splitting constants a and b in Figure 5 were determined from the equations representing the calculated values for the intermolecular shifts, Δ_1–Δ_4, shown in Figure 5, and the observed splittings among the three peaks of this region in Figure 3. These equations are

$$a = (28.0 + 3\Delta_3 - \Delta_1 - \Delta_2 - \Delta_4)/4$$
$$b = (8.4 + 3\Delta_4 - \Delta_1 - \Delta_2 - \Delta_3)/4 \qquad (14)$$

The enlarged spectra and the simulated ones are shown in Figure 6A–C for the pyrrole region and in Figure 7A–C for the ethyl region. The parameters used for the simulation spectra are given in Table III. From Figure 6 we see that in the pyrrole region of the spectrum the HMM and the 16-dipole methods reproduce both the single line of peak A and the small splitting observed for peak B. Both peak A and peak B are comprised of two peaks according to Figure 5, and it would appear that these lines must have rather large line widths. The splitting constants due to the quenching of the N–H tautomerism can be estimated from Table III, and the results are 14.6 ppm for the α-carbon and 9.5 ppm for the β-carbon atoms, respectively. These values are reasonable compared with those found for the system of tetraphenylporphyrin in solution.

As shown in Figure 7, all three methods are moderately successful in reproducing the ethyl region of the spectrum. The triplet shown in Figure 4B due to the methyl carbon atom could not be reproduced by the HMM method, even if the parameters were changed within an acceptable range. On the other hand, the 16-dipole method, as well as the JB method, can reproduce this triplet well, and the main features of the simulated spectrum resemble the observed one as shown. We now consider the methine region. The value of the splitting constant calculated by all three methods was approximately the same. The observed spectrum shows only a single line in the methine region. The average value calculated for the theoretical splitting was approximately 97 Hz, which is nearly equal to the observed line width.

As shown in Table III, all the parameters used in the simulation of the spectra fall in the reasonable range of values anticipated from the solution NMR studies of analogous system. Moreover, the crystallographic study shows that there is no significant change among the conformations of the subunits. These facts support the present proposed mechanisms.

Zn^{II}(OEP). Since this compound does not exhibit N–H tautomerism, the splitting in the signal of β-carbon in Figure 3b should be attributed to the ring-current effects. The three methods for calculating the ring-current effects yielded simulated spectra that reproduced the ethyl region of the spectrum satisfactorily. Only the JB method reproduced both the ethyl and the pyrrole regions well. Thus, we have chosen to restrict our discussion of the simulated spectra to the results obtained by the JB method. The spectrum simulated by using the JB method and the observed one are shown in Figure 8, parts A and B, respectively. The parameters used for the simulation are given in Table III. To obtain the spectrum shown in Figure 8A, the ring-current factor for the macro ring was reduced to about one-fourth of the value given in the literature.[19] The simulation spectrum for the pyrrole region was calculated by employing the same parameters as those used in the case of the OEP free base and assuming the same crystal structure, but with different line widths. The resulting simulated spectrum, along with the observed one for the pyrrole region, is shown in Figure 8C,D. If we employ larger line widths for the α-carbon peaks the simulated spectrum in Figure 8C agrees well with the observed one in Figure 8D. We could not reproduce the whole of the observed spectrum well using a single set of parameters. This result means that Zn^{II}(OEP) does not have the same crystal structure as that of OEP free base. However, the large splitting of the signal of β-carbon indicates that the symmetry

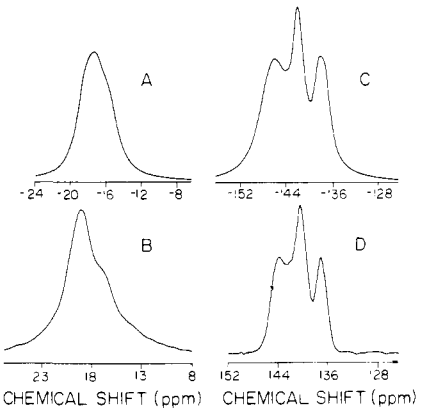

Figure 8. Comparison between simulated ^{13}C CP–MAS NMR spectra (A, C) and observed ones (B, D) for Zn^{II}(OEP) both in the ethyl region (A, B), and in the pyrrole region (C, D). Spectra A and C were calculated by the JB method making use of the parameters listed in Table III.

of the molecule as well as the environment in the crystalline state is lower than tetragonal.

Ni^{II}(OEP). We observed no splitting in the experimental spectrum of Ni^{II}(OEP). Since the crystal structure of this compound has the symmetry of S_4, the four pyrrole rings and four ethyl groups are mutually equivalent to each other. Thus there should be no splitting in the methine signal and two peaks at most in the signals of the other carbon atoms. As those splittings arise in the same subunit, they may be very small. This may be the reason why only a single peak is observed for each group of carbon atoms in the molecules.

Conclusion

The solid-state ^{13}C CP–MAS spectrum of free base OEP is reproduced well by the computer simulation, which takes into account both the intermolecular ring-current shielding and the quenching of the N–H tautomerism. The Haigh–Mallion and the 16-dipole methods are both quite successful in the simulation of the pyrrole region. These two methods and the Johnson–Bovey method are all moderately successful for the ethyl region. The sharp narrow line shape for the methine carbon could not be reproduced satisfactorily by any of the three methods. The parameters for the ring current used in the calculation of the spectra of OEP were larger than those that have been used previously for the porphyrin systems in liquid-phase NMR (see Table III).

The pyrrole region of the spectrum of Zn^{II}(OEP) was well reproduced by the same models and parameters used for the free base OEP. This means that the Zn^{II}(OEP) crystal has at most a 2-fold symmetry axis. The splitting in the ethyl region is much smaller than that observed for OEP. This fact suggests that the crystal structures of OEP and Zn^{II}(OEP) differ so that the ethyl group in the latter is not located above any ring of another molecule in the crystal.

The large line width of about 100 Hz observed in our spectra may be caused by the anisotropic magnetic susceptibility of the porphyrin crystals[32] as well as by the anisotropic part of the intermolecular ring-current shift (see eq 9).

Acknowledgment. This work was supported by a grant from the National Sciences and Engineering Council of Canada. We wish to thank Dr. A. Naito for many interesting discussions.

Appendix

To evaluate the intermolecular ring-current shifts, we need to employ vector calculations in the triclinic coordinates. The calculation of the inner products are easily accomplished by using the metric tensor; thus,

$$(\vec{A}\cdot\vec{B}) = (A_1A_2A_3)\begin{pmatrix} 1 & \cos\gamma & \cos\beta \\ \cos\gamma & 1 & \cos\alpha \\ \cos\beta & \cos\alpha & 1 \end{pmatrix}\begin{pmatrix} B_1 \\ B_2 \\ B_3 \end{pmatrix} \quad \text{(A1)}$$

where α, β, and γ are the angles between the triclinic axes of (2,3), (3,1), and (1,2), respectively. The outer product, which appears very frequently in the calculations, between the vectors A and B is expressed as follows

$$\vec{A}\times\vec{B} = (1/EN\sin\gamma)\cdot S\cdot S^{t}\cdot\begin{pmatrix} A_2B_3 - A_3B_2 \\ A_3B_1 - A_1B_3 \\ A_1B_2 - A_2B_1 \end{pmatrix} \quad \text{(A2)}$$

where

$$S = \begin{pmatrix} EN\sin\gamma & -EN\cos\gamma & EM\cos\gamma - \sin\gamma\cos\beta \\ 0 & EN & -EM \\ 0 & 0 & \sin\gamma \end{pmatrix} \quad \text{(A3)}$$

EM and EN are given by

$$EM = (\cos\alpha - (\cos\beta)(\cos\gamma))/\sin\gamma$$

$$EN = (\sin^2\beta - EM^2)^{1/2} \quad \text{(A4)}$$

Registry No. Zn^{II}(OEP), 17632-18-7; Ni^{II}(OEP), 24803-99-4; OEP, 2683-82-1.